PHYSICAL REVIEW C VOLUME 35, NUMBER 1 JANUARY 1987

Target and projectile excitation of $^{7}Li+^{11}B$, ^{13}C

J. Cook and A. K. Abdallah
Department of Physics, University of Petroleum and Minerals, Dhahran 31261, Saudi Arabia

M. N. Stephens and K. W. Kemper
Department of Physics, Florida State University, Tallahassee, Florida 32306
(Received 7 October 1986)

Angular distributions are reported for the excitation of states in ^{11}B and ^{13}C and the first excited state in ^{7}Li at a ^{7}Li energy of 34 MeV. Both distorted-wave Born approximation and coupled channels calculations are reported for these reactions. The projectile excitation is reasonably well described with a collective rotational model for ^{7}Li. For the excitation of states in ^{11}B, strong-coupling rotational, weak-coupling particle-rotation, and microscopic models are used. Weak-coupling particle-rotation and microscopic models are used for excitation of states in ^{13}C. In general, for the target excitation there is good agreement between the various calculations and the experimental data.

I. INTRODUCTION

This paper is one in a continuing series investigating the reactions between ^{6}Li or ^{7}Li and p-shell nuclei for incident energies around 30 MeV. Elastic scattering data for $^{6}Li+^{12}C$, ^{16}O (Ref. 1) and $^{7}Li+^{11}B$, ^{12}C, ^{13}C (Refs. 1 and 2) have been fitted with the optical model using Woods-Saxon and double-folded potentials. Several different Woods-Saxon potentials were found to fit each angular distribution well, except for $^{7}Li+^{11}B$, where it was not possible to obtain a good fit with Woods-Saxon potentials. The double-folded potentials were calculated by convoluting the M3Y effective nucleon-nucleon interaction with the ground state densities of the projectile and target nuclei. The potentials needed to be reduced in strength by about 30% in order to reproduce the data. Fits similar in quality to those using Woods-Saxon potentials were then obtained for ^{6}Li scattering and $^{7}Li+^{13}C$. The fits for $^{7}Li+^{12}C$ were slightly inferior, while those for $^{7}Li+^{11}B$ were much improved, particularly when the ground state quadrupole reorientation terms for ^{7}Li and ^{11}B were included in the calculations. Energy dependent average potentials of the Woods-Saxon form were also obtained for $^{6}Li+^{12}C$, $^{6}Li+^{16}O$, and $^{7}Li+^{12}C$.

Coupled channels calculations have been made for inelastic excitation of states in ^{6}Li (Refs. 3–5), ^{7}Li (Ref. 6), ^{12}C (Refs. 4–6), and ^{16}O (Refs. 4 and 5). Previously there had been little experimental data or few theoretical calculations for the excitation of unbound states of the projectile in a heavy-ion collision or for the excitation of states in both the projectile and target. Coupled-channels effects due to the 3^{+} 2.18 MeV state of ^{6}Li were found to be very important in the scattering of ^{6}Li projectiles. When coupling to this low-lying, strongly excited state was taken into account, two important results were observed. Firstly, the normalization of the real double-folded potential became significantly closer to unity, thus reducing the discrepancy between ^{6}Li and other heavy-ion projectiles, and secondly, the dominant imaginary potential became weaker in the surface region when the coupling was included. It was not possible to obtain a good description of the excitation of states in ^{7}Li from $^{7}Li+^{12}C$ scattering using coupled-channels calculations with deformed Woods-Saxon potentials.

Coupling to the 2^{+} 4.44 MeV state of ^{12}C had much the same effect in double-folded coupled channels calculations of $^{6}Li+^{12}C$ as coupling to the 3^{+} state of ^{6}Li, resulting in a change in the normalization of the potential and the strength of the imaginary potential.[4] The rotation-vibration model was applied to excitation of states in ^{12}C through $^{6}Li+^{12}C$ (Ref. 5) and $^{7}Li+^{12}C$ (Ref. 6) inelastic scattering with a fair degree of success. For $^{7}Li+^{12}C$ scattering, mutual excitation data were also measured, but it was not possible to describe these with DWBA or coupled channels calculations. A good description of the 3^{-} 6.13 MeV state of ^{16}O was obtained for $^{6}Li+^{16}O$ inelastic scattering using both double-folded[4] and Woods-Saxon[5] potentials.

Finite-range DWBA calculations have also been made for single-nucleon transfer reactions between ^{7}Li and ^{11}B, ^{12}C, ^{13}C targets.[2,6,7] In general the DWBA calculations were able to reproduce the shapes of the angular distributions well, and the spectroscopic factors obtained were in reasonable agreement with theoretical values and experimental values from light ion reactions. However, two problems in particular were noted and remain unsolved. Firstly, there is a phase shift of several degrees between the data and the calculations for the (^{7}Li,^{6}Li) and (^{7}Li,^{6}He) reactions, but not the (^{7}Li,^{8}Li) reaction, and, secondly, calculations involving a $2s_{1/2}$ transfer in the target nucleus are far too oscillatory compared with the experimental data.

In this paper we consider the inelastic scattering of $^{7}Li+^{11}B$ and $^{7}Li+^{13}C$ at 34 MeV, for both projectile and target excitation. New experimental data for the inelastic scattering of these systems are reported. Prior to this work the only reported data for $^{7}Li+^{11}B$ or $^{7}Li+^{13}C$ in-

 ©1987 The American Physical Society

elastic scattering were a single angular distribution by Schumacher *et al.*[8] The present projectile excitation data extend over the angular range of 15°—170° in the center-of-mass system and the target excitation data over the range 15°—95°. These data are analyzed in conjunction with previously reported[2] elastic scattering data which extend over the range 10°—170°. The analysis is carried out to be as consistent as possible with the preceding papers (Refs. 1—7) in this series. The calculations start from optical potentials determined from elastic scattering,[2] and then distorted-wave-Born-approximation (DWBA) calculations are made before progressing to coupled channels (CC) calculations.

For excitation of ^{7}Li a rotational model was assumed as in Ref. 5. The DWBA was not able to describe the projectile excitation data, making coupled channels calculations essential. A reasonable description of the data was then obtained. Excitation of states in ^{11}B was treated with both strong-coupling rotational and weak-coupling particle-rotational macroscopic models. The weak-coupling model was also used for ^{13}C. The strong-coupling model includes only members of the $K=3/2$ ground-state rotational band of ^{11}B, while the weak-coupling model treats the target nucleus as a particle (or hole) coupled to either the ground or first excited state of a ^{12}C core. A microscopic model was also used for both ^{11}B and ^{13}C. In this model the optical potential and form factors were calculated by convoluting a complex nucleon-nucleon interaction with the density distributions for the projectile and target nuclei. The target excitation data were well described, irrespective of the model used.

In Sec. II the experimental procedure used to measure the data is described. The analysis of the data is described in Secs. III, IV, and V for excitation of states in ^{7}Li, ^{11}B, and ^{13}C, respectively. In Sec. VI the conclusions are presented.

II. EXPERIMENTAL PROCEDURE

The experimental procedure used in this work has been described in considerable detail in Refs. 2 and 6, and only a brief outline will be given here. Beams of ^{7}Li, ^{11}B, and ^{13}C were accelerated with the Florida State University super FN tandem accelerator facility to 34 MeV ^{7}Li, 53.4 MeV for ^{11}B, and 63.1 MeV for ^{13}C. The actual incident energies were adjusted to yield the energies listed, at the center of the target. Self-supporting targets of ^{11}B and ^{13}C, enriched to 98% and 97%, respectively, and of areal densities of about 100 $\mu g/cm^2$ were bombarded by the ^{7}Li beam and the scattered ^{7}Li particles were detected. These measurements produced the forward angle data. Typical spectra for the forward angle measurements are shown in Fig. 1. The ^{7}Li targets were made by depositing natural Li metal (92.4% ^{7}Li) on Formvar backings. These targets were transferred under vacuum to avoid their turning to LiOH and dissolving in air. These targets were bombarded by beams of ^{11}B and ^{13}C and the recoil ^{7}Li particles were detected. These measurements resulted in the large angle elastic and inelastic ^{7}Li cross sections.

Standard $\Delta E \times E$ silicon surface barrier detectors were used and the particle identification was done via software

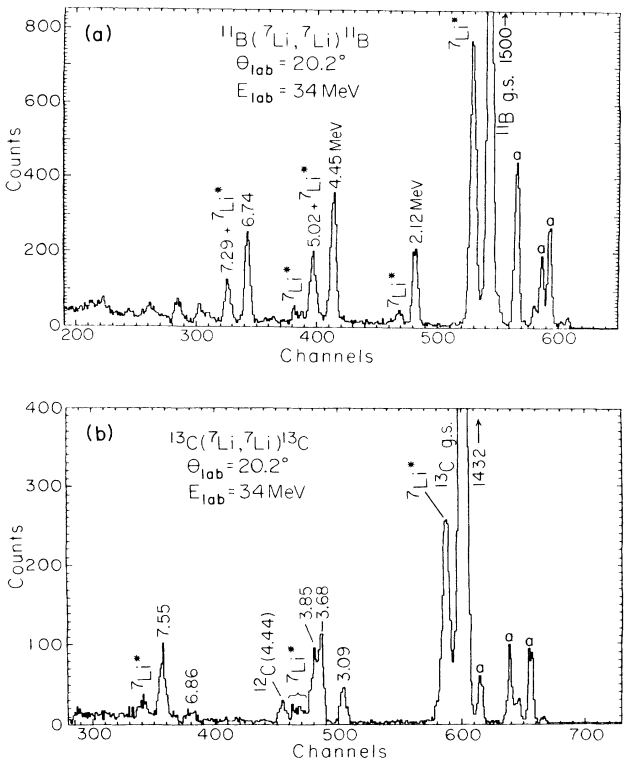

FIG. 1. Typical spectra for $^{7}Li+^{11}B$ and $^{7}Li+^{13}C$. The peaks labeled *a* are from target contaminants.

in the on-line data acquisition computer. The ^{11}B and ^{13}C target thicknesses were determined by scattering a 20 MeV ^{16}O beam from them and assuming the cross sections to be Rutherford. The absolute uncertainty in these measurements is ±11%.

The large angle cross sections were determined by overlapping the $^{7}Li+^{11}B$, ^{13}C measurements with those from ^{11}B, $^{13}C+^{7}Li$. The ^{11}B large angle elastic and inelastic scattering cross sections to the first excited state in ^{7}Li ($1/2^-$, 0.48 MeV) were determined to be a factor of 5 to 10 larger than those for ^{13}C and ^{12}C. To make certain of the relative large angle cross sections between the three targets, measurements were made at five angles where rapid switching between the beams of ^{11}B, ^{13}C, and ^{12}C occurred.

III. PROJECTILE EXCITATION

Distorted-wave Born approximation and coupled channels calculations were made for the excitation of the $1/2^-$, 0.48 MeV first excited state of ^{7}Li. The same procedure was followed for both ^{11}B and ^{13}C as targets.

In the DWBA calculations, the distorted waves were generated with the Woods-Saxon optical potentials which had previously[2] been found to fit the elastic scattering data. These are potentials II and V of Ref. 2 for $^{7}Li+^{11}B$ and $^{7}Li+^{13}C$, respectively, and are listed in Table I of the present work. The same distorting potentials were used in Ref. 2 for DWBA analyses of the single-nucleon transfer

TABLE I. Macroscopic potential parameters.

Target	Model	V (MeV)	r_R[a] (fm)	a_R (fm)	W (MeV)	r_I[a] (fm)	a_I (fm)
^{11}B	Optical model	184	0.62	0.76	6.54	1.39	0.74
	Projectile excitation	184	0.62	0.76	6.54	1.39	0.74
	Strong coupling	184	0.62	0.76	5.80[b] 6.05[c]	1.39	0.74
	Weak coupling	184	0.62	0.76	6.54	1.39	0.74
^{13}C	Optical model	159	0.63	0.81	8.16	1.33	0.78
	Projectile excitation	159	0.63	0.81	7.38	1.40	0.78
	Weak coupling[d]	159	0.63	0.81	7.30	1.33	0.78
	e	159	0.63	0.81	6.37	1.40	0.78

[a] $R_x = r_x(A_p^{1/3} + A_t^{1/3})$.
[b] Positive deformation length.
[c] Negative deformation length.
[d] Same deformation length for all states.
[e] Different deformation lengths for each state.

reaction data that were measured concurrently with the elastic and inelastic scattering data.

A strong-coupling rotational model was assumed for ^{7}Li with the $3/2^-$ ground state and the $1/2^-$ 0.48 MeV state being members of a $K=1/2$ band. Deformed Woods-Saxon form factors were used and Coulomb excitation was included. The same deformation lengths were used for the real and imaginary form factors and for the Coulomb excitation contributions. The results of the DWBA calculations and the optical model fits to the elastic scattering data are shown as the dashed lines in Figs. 2 and 3. A deformation length of 2.0 fm was required in the DWBA calculations to obtain the correct magnitude at forward angles. However, it was not possible to obtain the relative heights of the first and second maxima correctly, and also the DWBA calculations decreased too slowly in cross section for larger angles. For the ^{11}B target there did not seem to be a problem of phasing as had been observed earlier for projectile excitation of ^{7}Li by ^{12}C, in Ref. 6, although for the ^{13}C target there was still a shift in phase of the DWBA calculations relative to the data. This phasing difficulty in DWBA calculations of ^{7}Li projectile excitation has also been noted in other studies.[8–10]

In the coupled channels calculations the ground state reorientation contribution from ^{7}Li was also included. It was found unnecessary to change the potential parameters or the deformation length for the ^{11}B target, although for the ^{13}C target it was necessary to decrease the imaginary potential depth and to increase the imaginary radius parameter to obtain the best fit to the data. The coupled channels calculations are shown as the full lines in Figs. 2

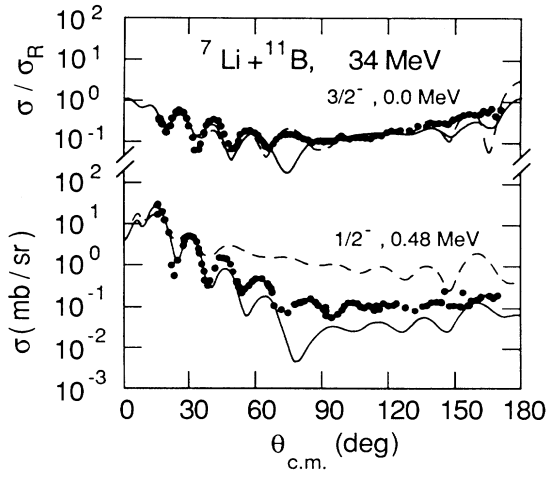

FIG. 2. Angular distributions for the elastic scattering of ^{7}Li+^{11}B at 34 MeV and for excitation of the $1/2^-$ 0.48 MeV state in ^{7}Li. The dashed lines are the results of an optical model fit to the elastic scattering data and of a DWBA calculation for the projectile excitation. Coupled channels calculations are shown as full lines.

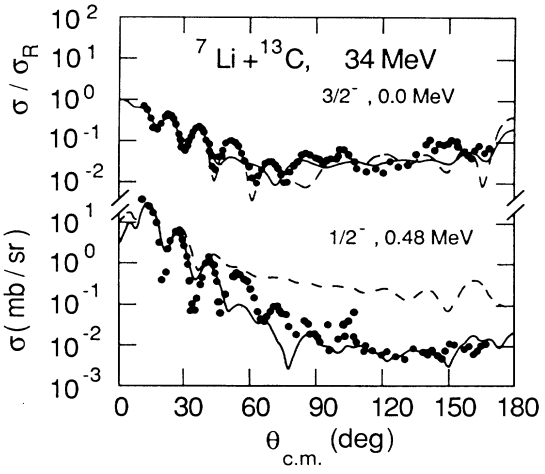

FIG. 3. Same as Fig. 1 except for ^{7}Li+^{13}C.

and 3, and the new potentials are listed in Table I under the heading of projectile excitation. For the ^{11}B target, the coupled channels calculations simultaneously describe fairly well the elastic scattering and projectile excitation data. There is a minimum in the elastic scattering prediction at about 70° whereas there is a maximum in the data, and the projectile excitation prediction is too low by a factor of about 2 for angles larger than 60°. However, the overall description of the data is good, particularly for the elastic scattering data at large angles where the ^{7}Li ground state reorientation contribution damps the oscillations in the calculations so that they are in better agreement with the data than the optical model calculations. For the ^{13}C target the description of both angular distributions is not as good. For both targets the description of the data is poor in the angular range of $\theta \approx 40°-80°$.

The deformation length of 2.0 fm found here for ^{7}Li is the same as that found from a study of $^{7}Li+^{12}C$ scattering at 34 MeV.[6] However, it is smaller than the value of 2.8 fm found from the $B(E2)$ value,[11] or of 3.5—4.5 fm found from DWBA analyses[8-10] of $^{7}Li+^{12}C$ inelastic scattering for energies of 36—79 MeV.

The comparative ease with which the projectile excitation was described with coupled channels calculations for ^{11}B and ^{13}C targets should be contrasted with the difficulty that was found[6] for a ^{12}C target. In the latter case, even after extensive parameter searching it was not possible to find a Woods-Saxon potential that would fit the projectile excitation well. Presumably the difficulty is related to the strongly excited 2^+ 4.44 MeV state of ^{12}C having a large effect on the elastic and projectile excitation channels, whereas the excited states of ^{11}B and ^{13}C are weakly excited in comparison and have less of an effect.

IV. EXCITATION OF STATES IN ^{11}B

The states excited strongly enough in ^{11}B to extract angular distributions are the $3/2^-$ ground state, and the $1/2^-$ 2.12 MeV, $5/2^-$ 4.45 MeV, $3/2^-$ 5.02 MeV, and $7/2^-$ 6.74 MeV states. Data (Fig. 4) were also measured for the $5/2^+$ 7.29 MeV and $5/2^-$ 8.92 MeV states of ^{11}B, but have not been analyzed in this work. In a simple rotational description[12,13] the ground state forms a $K=3/2$ rotational band with the $5/2^-$ and $7/2^-$ excited states, while the $1/2^-$ and $3/2^-$ states are members of a rotational band with $K=1/2$. The selection rule for K for rotational excitations forbids collective transitions between the bands with $K=3/2$ and $K=1/2$ and only allows transitions to occur within each band. If this selection rule were strictly true, the cross sections for states with $K=1/2$ would be much smaller than those with $K=3/2$, whereas experimentally their magnitudes are very similar. In fact, the particle-rotation coupling term in the Hamiltonian mixes configurations with the same angular momentum but with $\Delta K=\pm 1$. Thus both $3/2^-$ states and the $5/2^-$, $7/2^-$ states of ^{11}B have $K=1/2$ and $K=3/2$ components of approximately equal amplitude. Calculations with K-band mixing have been made[13] for $^{3}He+^{11}B$ inelastic scattering, but the results for the ground state band did not differ significantly with and without K-band mixing.

Instead of describing the low-lying negative-parity states of ^{11}B as mixtures of $K=1/2$ and 3/2 rotational bands, an equivalent method derived by Clegg[14] is to express the wave functions as a sum of terms consisting of the wave function of a member of the ground state rotational band of ^{12}C coupled to a $1p_{3/2}$ or $1p_{1/2}$ proton hole. The leading terms show that the ground state has the structure of a ^{12}C core in its ground state coupled with a $1p_{3/2}$ hole, and the $1/2^-,3/2^-,5/2^-,7/2^-$ excited states are due to a $1p_{3/2}$ hole coupled to a ^{12}C core in its 2^+ first excited state. This model, here termed the weak-coupling model, has also been used in the present description of $^{7}Li+^{11}B$ inelastic scattering.

Finally, calculations are made for excitation of states in ^{11}B using microscopic transition densities from the $(1s)^4(1p)^7$ intermediate coupling model calculations of Cohen and Kurath.[15] Here, the excited states arise from transition between the $1p_{1/2}$ and $1p_{3/2}$ nucleons.

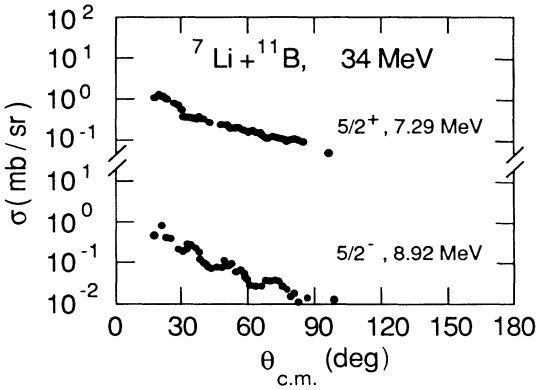

FIG. 4. Experimental data for $^{7}Li+^{11}B$ inelastic scattering at 34 MeV for excitation of the $5/2^+$ 7.29 MeV and $5/2^-$ 8.92 MeV states of ^{11}B.

A. Strong coupling model

The $3/2^-$ ground state and the $5/2^-$ 4.45 MeV and $7/2^-$ 6.74 MeV states of ^{11}B are assumed to be members of a $K^{\pi}=3/2^-$ rotational band based upon the ground state of ^{11}B and are treated with the strong coupling rotational model. The form factors required in this model have been described in detail in Ref. 5.

Firstly, DWBA calculations were made using the optical model potential parameters of Table I. The results of these calculations are shown as the dashed lines in Fig. 5. Only quadrupole transitions were considered and a deformation length of $|\delta_2|=1.0$ fm employed. Coulomb excitation was included, with the same deformation length as the nuclear part of the potential. For the $5/2^-$ state the DWBA calculation has the correct magnitude at the first peak in the angular distribution, but the slope is too small, so that at larger angles the cross sections are larger than the data. With a deformation length of 1.0 fm the forward angle cross sections for the $7/2^-$ state are too small, but the problem with the slope is even greater here, so that

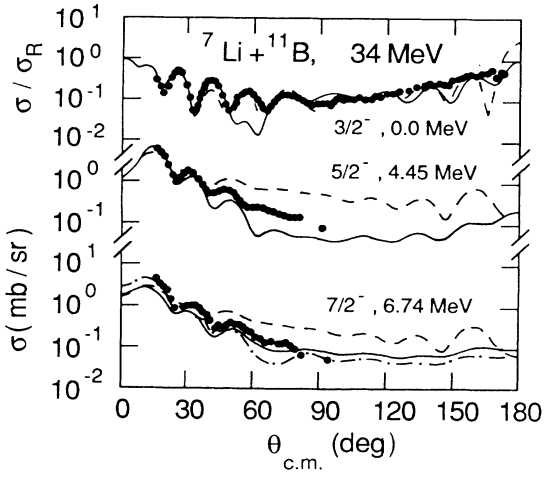

FIG. 5. Experimental data and calculations for excitation of states in ^{11}B via the ^{11}B(^{7}Li,^{7}Li)^{11}B* reaction at 34 MeV. A strong coupling rotational model is assumed for ^{11}B. The dashed lines are the results of an optical model fit to the elastic scattering data and of DWBA calculations for the target excitation. Coupled channels calculations using a negative deformation length are shown as full lines. The dash-dot line indicates the effect of using a different deformation length for the $3/2^- \rightarrow 7/2^-$ transition compared with the $3/2^- \rightarrow 5/2^-$ transition.

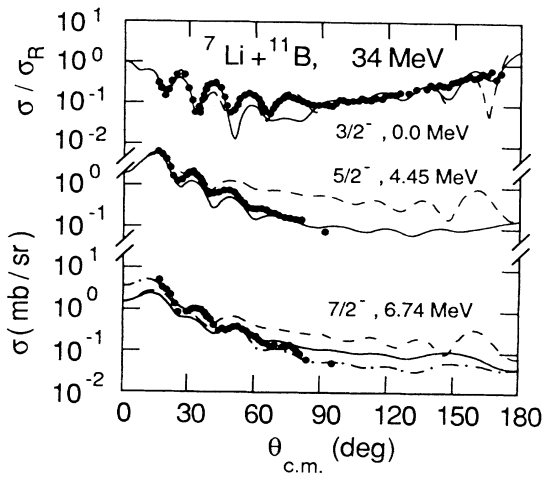

FIG. 6. Same as Fig. 5 except a positive deformation length was used.

the predicted cross sections are still too large at larger angles.

In the coupled channels calculations, quadrupole transitions were included between the $3/2^-$ and $5/2^-$ states, the $3/2^-$ and $7/2^-$ states, and the $5/2^-$ and $7/2^-$ states. Quadrupole reorientation was included for the ground state, but not for the excited states, since it was found to have a negligible effect. Couplings with $l=4$ were also found to be unimportant. Calculations were first made with the same negative value of δ_2 for all transitions: $\delta_2=-1.20$ fm. The results of these calculations are shown as the full lines in Fig. 5. The magnitude of δ_2 was determined principally by the forward angle fit to the $5/2^-$ data. It was necessary to reduce the strength of the imaginary potential by about 10% to obtain the best fit to the data, and the description of the elastic scattering worsened in the angular range 50°–90° relative to the optical model fit. The data for the $5/2^-$ state were well described in shape and magnitude, but the cross sections for the $7/2^-$ state still had the wrong slope. By omitting the $3/2^- \rightarrow 7/2^-$ and $5/2^- \rightarrow 7/2^-$ couplings in turn we determined that the $7/2^-$ state is mainly excited through the $3/2^- \rightarrow 7/2^-$ direct transition. Changing the deformation length for this transition to -1.65 fm resulted in the correct magnitude and slope for the $7/2^-$ state, as shown by the dash-dot lines in Fig. 5.

The same calculations were repeated for a positive deformation length and resulted in a reduced χ^2, arising mainly from an increase in the cross section for the $5/2^-$ state for $\theta > 60°$. The fits to the data are shown in Fig. 6. A value of $\delta_2=+1.0$ fm resulted in the optimum fit when applied to all the transitions, although for the best description of the $7/2^-$ state it was necessary to use a value of $\delta_2=+1.40$ fm for the $3/2^- \rightarrow 7/2^-$ transition.

The deformation lengths for ^{11}B are summarized in Table II. From the coupled channels calculations described here a quadrupole deformation length $\delta_2=-1.20$ fm or $+1.00$ fm is obtained for excitation of the $5/2^-$ state and $\delta_2=-1.65$ fm for the $7/2^-$ state in ^{11}B via ^{7}Li inelastic scattering. Shahabuddin *et al.*[13] obtained δ_2 $(=\beta_2 R_R)=-1.12$ fm at 17.5 MeV and $\delta_2=-1.46$ fm at 40 MeV for ^{3}He+^{11}B inelastic scattering using the no-K-band mixing model. Very similar

TABLE II. Deformation lengths δ_2 for strong-coupling transitions in ^{11}B.

State	p[a] 30 MeV	^{3}He[b] 17.5, 40 MeV	^{3}He[c] 17.5 MeV	^{3}He[c] 40 MeV	^{7}Li[d] 34 MeV
$5/2^-$ 4.45 MeV	1.0–2.0	−1.30	−1.12	−1.46	−1.20/+1.00
$7/2^-$ 6.74 MeV	1.0–2.0	−1.35	−1.12	−1.46	−1.65/+1.40

[a]DWBA, Ref. 17.
[b]DWBA, Ref. 16.
[c]CC, Ref. 13.
[d]CC, the present work.

values were found if K-band mixing was included or if $\delta_2=\beta_2 R_I$ was assumed. In their study it was found possible to use the same deformation length for all states, but in a previous study[16] of the same data using the DWBA, $\delta_2=-1.03$ fm for the $5/2^-$ state and $\delta_2=-1.35$ fm for the $7/2^-$ state were required at both energies. The coupled channels calculations[13] of Shahabuddin *et al.* produced a definite preference for a negative deformation length. In the present work there is a slight preference for a positive deformation length, but the difference in the quality of fits between using positive and negative deformation lengths does not allow a definite decision to be made. For p+^{11}B at 30 MeV a DWBA analysis[17] gives different deformation lengths for each of the five low-lying negative parity states with values in the range $|\delta_2|=1.0$–2.0 fm. It would seem, therefore, that in general the present results are consistent with previous studies.

B. Weak coupling model

In the weak coupling model used here it is assumed that the first five negative-parity states of ^{11}B can be constructed from the coupling of a proton hole to the ground state rotational band of a ^{12}C core. This is also known as the unified model. Clegg[14] has derived expressions for the wave functions of ^{11}B using this model as a sum of terms involving the coupling of a $1p_{3/2}$ or $1p_{1/2}$ hole to the 0^+, 2^+, and 4^+ members of the ground state rotational band. In the present calculations only the leading terms in the sum have been used. It is then assumed that the ground state of ^{11}B is formed from the coupling of a $1p_{3/2}$ hole with the 0^+ ground state of ^{12}C and the $1/2^-$, $5/2^-$, $3/2^-$, and $7/2^-$ sequence of excited states from the coupling of a $1p_{3/2}$ hole with the 2^+ first excited state of ^{12}C.

The formalism and notation for the form factor required for weak coupling model calculations with the computer code CHUCK3 (Ref. 18) follows that of Ref. 5. It is assumed that the initial state of spin I_α in channel α is comprised of the coupling of a single particle wave function of total angular momentum j_α to a rotational core wave function of total angular momentum J_α and body-fixed component K_α so that the wave function is given by

$$|I_\alpha M_\alpha\rangle=[\phi_{j_\alpha}|K_\alpha J_\alpha\rangle]^{M_\alpha}_{I_\alpha} . \quad (1)$$

The final state in channel β is formed similarly. The potential is assumed to have the Woods-Saxon form

$$V(r,\Omega')=V_0/\left[1+\exp\left[\frac{r-R'(\Omega')}{a}\right]\right] , \quad (2)$$

where Ω' refers to a frame fixed in the body of the core. It is assumed for rotational excitations of the core within the ground state band that the potential is deformed according to

$$R(\Omega')=R_0+\sum_\lambda \delta_\lambda Y_{\lambda 0}(\Omega') . \quad (3)$$

Then the form factor for CHUCK3 (Ref. 18) is

$$F_{l0l}(r)=\delta_{j_\beta,j_\alpha}\delta_{K_\beta,K_\alpha}(-)^l(-)^{j_\alpha+l-J_\beta-I_\alpha} \times i^{l+[\alpha]-[\beta]}\hat{S}_\beta\hat{I}_\alpha\hat{I}_\beta\hat{J}_\alpha \times\langle J_\alpha l K_\alpha 0|J_\beta K_\alpha\rangle W(J_\alpha I_\alpha J_\beta I_\beta|j_\alpha l)v_l^0(r) , \quad (4)$$

where

$$v_l^0(r)=\int V(r,\Omega')Y_{l0}(\Omega')d\Omega' . \quad (5)$$

Firstly, DWBA calculations were made, using the optical model potential parameters of Table I. Only quadrupole transitions were considered and a deformation length of $\delta_2=-1.40$ fm employed. This value was found previously from a coupled channels analysis[6] of ^{7}Li+^{12}C inelastic scattering at 34 MeV. Coulomb excitation was included, with the same deformation length as the nuclear part of the potential. The results of these calculations are shown as the dashed lines in Fig. 7. They have the correct forward angle magnitude but decrease too slowly relative to the data for increasing angles and therefore become too large in magnitude for $\theta>30°$.

When coupled channels calculations are made, including the reorientation terms, the slopes of the theoretical predictions now agree well with the data, although there is still some problem for the $3/2^-$, 5.02 MeV state. The description of the elastic scattering is improved for the peak around 40°, but it was not possible to obtain the

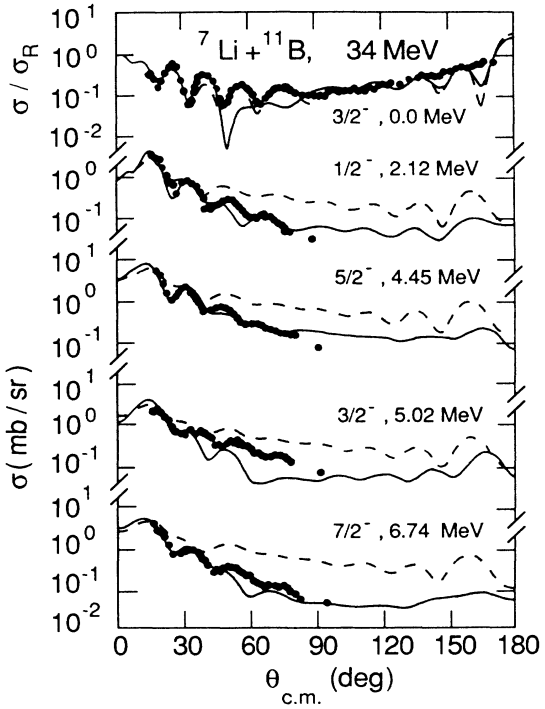

FIG. 7. Experimental data and calculations for ^{11}B(^{7}Li,^{7}Li)^{11}B* inelastic scattering at 34 MeV. A weak coupling particle-rotational model was assumed for ^{11}B. The dashed lines are the results of an optical model fit to the elastic scattering data and of DWBA calculations for the target excitation. Coupled channels calculations are shown as full lines.

correct structure in the angular distribution for $\theta=50°-90°$. In the coupled channels calculations the deformation parameter had to be changed to -1.709 fm to obtain the correct magnitude of the inelastic states, but no other changes in the potential parameters were necessary. This deformation length is still larger than that found[13] for ^{3}He+^{11}B inelastic scattering, but is within the range of values found for p+^{11}B (Ref. 17). It would appear necessary to include all the low-lying negative parity states in a coupled channels calculation to obtain a single deformation length independent of state.

C. Microscopic model

The states that were analyzed in the preceding subsection with the weak coupling model were also analyzed with a microscopic model. In this model the optical potential for elastic scattering and the form factors for the inelastic transitions are calculated by integrating an effective nucleon-nucleon interaction over the density distributions for the projectile and target nuclei. The method is reviewed in general in Refs. 19–21, and the particular formalism that is used in this paper is described in detail in Ref. 22. The form factor $F^{\rm CH}$ required for the computer program CHUCK3 (Ref. 18) is related to the form factor F of Ref. 22 by

$$F^{\rm CH}_{lsj}(R)=\hat{s}\,\hat{s}_\beta\hat{I}_\beta F^{lsj}(R)\ . \tag{6}$$

An additional difference is that instead of using spectroscopic amplitudes $S^J_{TM}(j_fj_i)$ as in Ref. 22, in this paper spectroscopic amplitudes $Z_{\rm p/n}(j_fj_i)$ are used. They are defined in Ref. 23 and the relation between them is

$$S^J_{\substack{00\\10}}(j_fj_i)=\frac{\hat{j}_f\hat{J}_i}{\hat{J}_f}[Z^J_{\rm N}(j_fj_i)\pm Z^J_{\rm p}(j_fj_i)]\ . \tag{7}$$

The real part of the effective nucleon-nucleon interaction was taken from the work of Bertsch *et al.*[24] Single-nucleon knockout exchange was approximated by inclusion of a zero-range pseudointeraction.[25] The most important component of the interaction for the case under study was that part with $S=0$ and $T=0$. Its explicit form was

$$v^0_{00}(s)=7999\frac{e^{-4s}}{4s}-2134\frac{e^{-2.5s}}{2.5s}-390\delta(s)\ . \tag{8}$$

The real optical potentials and form factors were multiplied by a parameter N_R which could be varied to improve the fits to the data. To avoid using a microscopic model for the real parts of the optical potentials and form factors and a different model for the imaginary parts, an empirical imaginary interaction was used to calculate the imaginary parts. The imaginary interaction had the form

$$w(r)=-N_Ie^{-\gamma r^2}\ , \tag{9}$$

with the parameters N_I and γ determined from fitting the experimental data.

Cohen and Kurath[15] transition densities for ^{7}Li and ^{11}B were used. Harmonic oscillator radial wave functions were used with $\alpha=0.578$ fm^{-1} for ^{7}Li (Ref. 23), and $\alpha=0.605$ fm^{-1} for ^{11}B (Ref. 26). For the projectile only the $J=0$ monopole ground state density was used since the computer code could not accommodate the full spin formalism of a spin 3/2 projectile and excitations of a spin 3/2 target. The spectroscopic amplitudes for ^{7}Li are listed in Table III of Ref. 23. The spectroscopic amplitudes for ^{11}B are listed in our Table III. For the ground state both the $J=0$ monopole and $J=2$ quadrupole densities were included, but for the inelastic transitions only the $J=2$ terms were employed.

TABLE III. Spectroscopic amplitudes $Z^J_{\rm p/n}(j_fj_i)$ for transitions in ^{11}B. (For the $3/2^-_1\rightarrow 3/2^-_1$ transition the amplitude for $1s_{1/2}1s^{-1}_{1/2}$ had $Z_{\rm n}=Z_{\rm p}=1.414$ with $J=0$.)

		$1p_{1/2}1p^{-1}_{1/2}$		$1p_{3/2}1p^{-1}_{1/2}$		$1p_{1/2}1p^{-1}_{3/2}$		$1p_{3/2}1p^{-1}_{3/2}$	
Transition	J	p	n	p	n	p	n	p	n
$3/2^-_1\rightarrow 3/2^-_1$	0	0.262	0.525	0.000	0.000	0.000	0.000	1.315	1.628
	1	−0.058	0.058	0.075	0.028	−0.075	−0.028	0.427	0.073
	2	0.000	0.000	−0.079	−0.107	0.079	0.107	−0.373	−0.031
	3	0.000	0.000	0.000	0.000	0.000	0.000	0.393	0.007
$3/2^-_1\rightarrow 1/2^-$	1	0.000	−0.003	0.183	−0.017	−0.240	−0.009	0.016	−0.015
	2	0.000	0.000	−0.120	0.141	−0.239	−0.186	0.099	0.105
$3/2^-_1\rightarrow 5/2^-$	1	0.174	−0.010	−0.054	0.012	−0.278	0.060	−0.037	−0.015
	2	0.000	0.000	0.169	0.174	−0.504	−0.254	0.066	0.051
	3	0.000	0.000	0.000	0.000	0.000	0.000	0.067	0.013
$3/2^-_1\rightarrow 3/2^-_2$	0	0.132	−0.024	0.000	0.000	0.000	0.000	−0.093	0.017
	1	0.057	−0.068	0.058	−0.006	0.392	0.031	0.061	−0.058
	2	0.000	0.000	0.090	0.141	−0.081	−0.220	−0.013	0.108
	3	0.000	0.000	0.000	0.000	0.000	0.000	0.148	0.021
$3/2^-_1\rightarrow 7/2^-$	2	0.000	0.000	−0.173	−0.207	−0.041	0.437	−0.126	−0.147
	3	0.000	0.000	0.000	0.000	0.000	0.000	0.021	0.032

The first step was to fit the elastic scattering data to determine the normalization N_R of the real potential and the strength N_I and range γ of the imaginary potential. Only the spherical parts of the potentials were used. The calculations were carried out with the optical model code HERMES.[27] The range parameter γ was varied in steps of 0.01 fm^{-2} and for each value of γ the code determined the best values of N_R and N_I from a least squares fitting routine. The optimum value of γ was that which gave the smallest χ^2. The parameters for the best optical model fit were $N_R=0.57$, $N_I=1.24$ MeV, and $\gamma=0.195$ fm^{-2}. The result of the fit is shown as the dashed line in Fig. 7. It is quite acceptable out to 110°, but does not correctly describe the data at angles larger than this.

DWBA calculations were now made for excitation of states in ^{11}B and are shown as the dashed lines in Fig. 8. The cross sections for the $1/2^-$ 2.12 MeV, $5/2^-$ 4.45 MeV and $7/2^-$ 6.74 MeV states had the correct magnitude and rate of falloff, but the cross section for the $3/2^-$ 5.02 MeV state was too small and had to be multiplied by a factor of 2.4 to agree with the data.

For the coupled channels calculations quadrupole reorientation in the ground state of ^{11}B was included. This improved the fit to the large angle elastic scattering data, but had a negligible effect on the inelastic cross sections. To obtain the best overall fits it was necessary to change N_I to 1.95 MeV, but changes in N_R or γ made the fits deteriorate in quality. The form factors for the $5/2^-$ 4.45 MeV and $3/2^-$ 5.02 MeV states had to be multiplied by 0.65 and 1.2, respectively, to produce cross sections of the correct magnitude. The results of the coupled channels calculation are shown as the full lines in Fig. 8. They are in good agreement with the experimental data and there is little difference compared with the DWBA calculations for angles smaller than 100°.

In conclusion, the microscopic model used here with Cohen-Kurath[15] transition densities is successful in describing the inelastic excitation of states in ^{11}B, apart from some normalization differences.

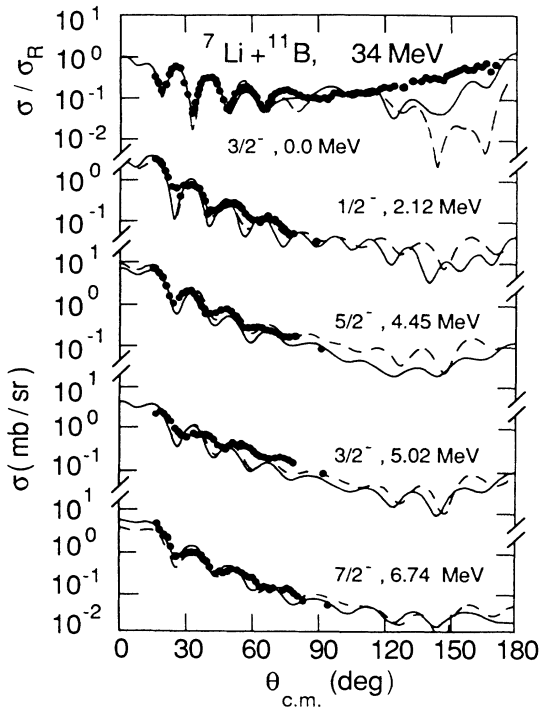

FIG. 8. Experimental data and calculations for $^{11}B(^{7}Li,^{7}Li)^{11}B^*$ inelastic scattering at 34 MeV. The potentials and form factors were calculated using a microscopic model. The dashed lines are the results of an optical model fit to the elastic scattering data and of DWBA calculations for the target excitation. Coupled channels calculations are shown as full lines.

V. EXCITATION OF STATES IN ^{13}C

Experimental data were measured for the $1/2^-$ ground state and the $1/2^+$ 3.09 MeV, $3/2^-$ 3.68 MeV, and $5/2^-$ 7.55 MeV excited states. In the weak-coupling model the ground state of ^{13}C has the structure of a $1p_{1/2}$ neutron coupled to a ^{12}C core in its ground state, while the doublet of $3/2^-$ and $5/2^-$ excited states arise from the coupling of a $1p_{1/2}$ neutron to a ^{12}C core in its 2^+ first excited state. This model is used here to analyze the $1/2^-$-$3/2^-$-$5/2^-$ sequence of states. It had previously been applied to proton,[28] deuteron,[29] and pion[30] inelastic scattering from ^{13}C. In a macroscopic model the $1/2^+$ 3.09 MeV state could be considered as a 1^- vibration of a ^{12}C core weakly coupled to a $1p_{1/2}$ neutron. However, it has been shown (e.g., Ref. 31) that a microscopic model is more applicable here.

In a microscopic model the $1/2^-$, $3/2^-$, and $5/2^-$ states have a $(1s)^4(1p)^9$ shell model structure with the excited states arising from transitions between the $1p_{1/2}$ and $1p_{3/2}$ nucleons. The $1/2^+$ 3.09 MeV state arises principally from a neutron $2s_{1/2}1p_{1/2}^{-1}$ single particle transition. There have been many previous studies of inelastic scattering of various projectiles from ^{13}C using microscopic wave functions (e.g., Refs. 28–35).

A. Weak coupling model

The weak coupling model that was described in Sec. IV B was also applied in the analysis of several low lying states in ^{13}C. It is assumed that the $1/2^-$ ground state of ^{13}C arises from the coupling of a $1p_{1/2}$ neutron with a ^{12}C

TABLE IV. Deformation lengths δ_2 for weak-coupling transitions in ^{13}C.

State	p[a] 800 MeV	d[b] 13 MeV	^{7}Li[c] 34 MeV	π[d] 162 MeV
$3/2^-$ 3.68 MeV	1.44	1.23	−1.30	1.2±0.1
$5/2^-$ 7.55 MeV	1.23		−1.00	1.1±0.1

[a]DWBA, Ref. 28.
[b]CC, Ref. 29. A vibrational excitation was assumed for excitation of the ^{12}C core.
[c]CC, the present work.
[d]DWIA, Ref. 30.

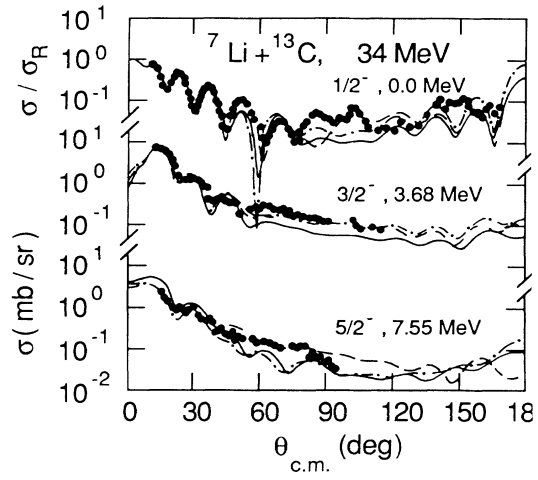

FIG. 9. Experimental data and calculations for ^{13}C(^{7}Li,^{7}Li)^{13}C* inelastic scattering at 34 MeV. A weak coupling particle-rotation model was assumed for ^{13}C. The dashed lines are the results of an optical model fit to the elastic scattering data and of DWBA calculations for the target excitation. Coupled channels calculations with the same deformation length for each state are shown as full lines. The dash-dot lines correspond to coupled channels calculations with different deformation lengths for each state.

core in its ground state, and that the $3/2^-$ 3.68 MeV and $5/2^-$ 7.55 MeV states of ^{13}C arise from the coupling of a $1p_{1/2}$ neutron with a ^{12}C core in its 2^+ 4.44 MeV first excited state.

Firstly, DWBA calculations were made using the optical model potential parameters of Table I. Only quadrupole transitions were considered, and Coulomb excitation was included, with the same deformation length as the nuclear part of the potential. A deformation length of $\delta_2 = -1.30$ fm was found to produce cross sections for inelastic scattering in good agreement with the data for the $3/2^-$ and $5/2^-$ states. The results of these calculations are shown as the dashed lines in Fig. 7.

Starting from the optical potential and the deformation length $\delta_2 = -1.30$ fm, coupled channels calculations were now made. The $l=2$ coupling between the $3/2^-$ and $5/2^-$ states was included, as well as reorientation. To obtain the best overall fit to the data it was necessary to decrease W and r_I for the imaginary potential. The results of these calculations are shown as the full lines in Fig. 9. The fit to the elastic scattering deteriorated, as is usual in coupled channels calculations. The cross sections for the $3/2^-$ states are the same as before for $\theta < 50°$, but are a little too small for larger angles. The calculated cross sections for the $5/2^-$ state are too large for $\theta < 40°$ and too small for $\theta > 40°$. This latter problem was partly overcome by changing the deformation length for the $1/2^- \rightarrow 5/2^-$ transition to -1.00 fm. It was then necessary to readjust the potential parameters again (Table I) for the best overall fit shown as the dash-dot lines. The fit to the $3/2^-$ state now improved for $\theta > 50°$, and to the $5/2^-$ state for $\theta < 40°$. However, it was not possible to obtain the magnitude of the cross sections correctly for the $5/2^-$ state for $\theta > 40°$ with this procedure. Thus the DWBA gives a better description of the excitation to this state than the coupled channels method.

The deformation lengths found here for ^{7}Li+^{13}C inelastic scattering are compared in Table IV with those from other analyses. For the $3/2^-$ state the value found here of -1.30 fm is within the range $|\delta_2| = 1.20$—1.44 fm found from proton,[28] deuteron,[29] and pion[30] inelastic scattering. Our value of -1.00 fm for the $5/2^-$ state is a little smaller than the values of 1.10—1.23 fm found from the other studies. The various studies, however, are in agreement that the deformation length for the $5/2^-$ state is smaller than that for the $3/2^-$ state.

B. Microscopic model

The microscopic model that was described in Sec. IV C was also applied to the analyses of states in ^{13}C. The same density as before was used for ^{7}Li. For excitations to negative parity states in ^{13}C, Cohen and Kurath[15] transition densities were used with the spectroscopic amplitudes of Table V. The transition from the ground state to the $1/2^+$ 3.09 MeV state is primarily due to a neutron $2s_{1/2}1p_{1/2}^{-1}$ transition. The spectroscopic amplitudes for excitation of this state were taken from Collins *et al.*[33] and are listed in Table VI. Harmonic oscillator radial wave functions were used for ^{13}C with $\alpha = 0.605$ fm^{-1}.

Firstly, the elastic scattering data were fitted using the procedure described in Sec. IV C. The parameters that resulted in the optimum fit were $N_R = 0.50$, $N_I = 0.51$ MeV, and $\gamma = 0.112$ fm^{-2}. The result of the fit is shown as the dashed line in Fig. 9. As with the microscopic

TABLE V. Spectroscopic amplitudes $Z^J_{p/n}(j_f j_i)$ for transitions to negative parity states in ^{13}C. (For the $1/2^-_1 \rightarrow 1/2^-_1$ transition the amplitude for $1s_{1/2}1s_{1/2}^{-1}$ had $Z_n = Z_p = 1.414$ with $J=0$.)

		$1p_{1/2}1p_{1/2}^{-1}$		$1p_{3/2}1p_{1/2}^{-1}$		$1p_{1/2}1p_{3/2}^{-1}$		$1p_{3/2}1p_{3/2}^{-1}$	
Transition	J	p	n	p	n	p	n	p	n
$1/2^-_1 \rightarrow 1/2^-_1$	0	0.339	0.800	0.000	0.000	0.000	0.000	1.760	1.934
$1/2^-_1 \rightarrow 3/2^-_1$	1	−0.071	−0.001	0.025	0.263	−0.012	−1.158	0.113	−0.135
	2	0.000	0.000	−0.674	0.066	1.187	1.496	−0.318	−0.076
$1/2^-_1 \rightarrow 5/2^-_1$	2	0.000	0.000	−0.681	−0.539	1.937	−0.002	−0.318	−0.128
	3	0.000	0.000	0.000	0.000	0.000	0.000	0.088	−0.055

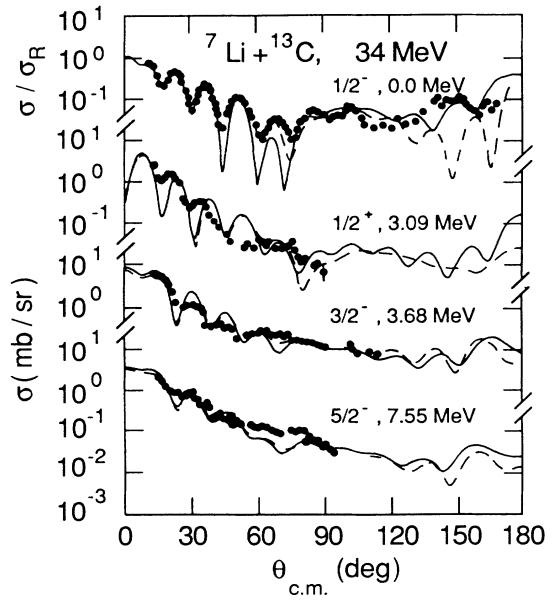

FIG. 10. Experimental data and calculations for ^{13}C(^{7}Li,^{7}Li)^{13}C* inelastic scattering at 34 MeV. The potentials and form factors were calculated using a microscopic model. The dashed lines are the results of an optical model fit to the elastic scattering data and of DWBA calculations for the target excitation. Coupled channels calculations are shown as full lines.

description of the ^{7}Li+^{11}B elastic scattering data, the fit is quite reasonable for angles less than 120°, but is poor for angles larger than this.

Microscopic DWBA calculations were now made for excitation of states in ^{13}C and are shown as the dashed lines in Fig. 9. The calculated cross sections for the $1/2^+$ 3.09 MeV and $3/2^-$ 3.68 MeV states had the correct magnitude, but for the $5/2^-$ 7.55 MeV state had to be multiplied by 0.73 to obtain agreement with the magnitude of the expermental data at forward angles. Coupled channels calculations were now performed. In these the form factor for excitation of the $5/2^-$ 7.55 MeV state was multiplied by 0.85 on the basis of the DWBA calculations to obtain the correct magnitude of the cross sections for this state. It was necessary to adjust the depth of the imaginary interaction to $N_I = 0.73$ MeV to obtain the best fits to the data with the coupled channels calculations. These fits are shown as the full lines in Fig. 10.

The description of the elastic scattering at large angles is improved by using the coupled channels formalism compared with a one-channel optical model, but the oscillations around 60°—70° are too deep. The differences between DWBA and coupled channels are insignificant for the excited states within the angular range of the data ($\theta < 100°$), although for larger angles the DWBA prediction for the $1/2^+$ state shows cross sections varying smoothly whereas they are oscillatory in the coupled channels calculations. The general description of the data for the $3/2^-$ and $5/2^-$ states is fairly reasonable, but there is a phase shift of about 4° between the calculations and the experimental data for the $1/2^+$ state. Ohnuma *et al.*[36] recently made a comparative study of the ^{13}C(p,p')^{13}C and ^{13}C(p,n)^{13}N reactions at a proton energy of 35 MeV. They carried out a microscopic DWBA analysis using Cohen and Kurath[15] wave functions for the negative parity states and from the Millener and Kurath interaction[37] for the positive parity states. Good fits to the data for the $1/2^-$ ground state and the $3/2^-$ and $5/2^+$ excited states of both ^{13}C and ^{13}N were obtained. The $1/2^+$ state of ^{13}C was not even qualitatively reproduced, although the calculations for its analog in ^{13}N were in good agreement with the data. The authors concluded that the source of the problem must lie in the shell-model calculations since otherwise the (p,n) calculations would not be in agreement with the data. Since the (p,n) reaction is determined by the isovector part of the wave function and is presumably fairly correct, the problem is likely to be with the isoscalar part of the interaction. It is therefore concluded that the $3/2^-$ and $5/2^-$ states of ^{13}C are well described by the microscopic calculations presented here, but that there are some discrepancies for the $1/2^+$ state.

VI. CONCLUSIONS

New experimental data have been measured for ^{7}Li+^{11}B and ^{7}Li+^{13}C inelastic scattering at 34 MeV. The data, both for projectile and target excitation, have been analyzed with DWBA and coupled channels calculations. For the projectile excitation, due to the strong coupling involved, there is a large discrepancy between the DWBA calculations and the data and therefore coupled channels calculations are necessary. There is little difference between the DWBA and coupled channels calculations for the target excitation on account of the weaker coupling of these states.

TABLE VI. Spectroscopic amplitudes $Z^J_{p/n}(j_f j_i)$ for excitation of the $1/2^+$ 3.09 MeV state in ^{13}C.

		J	p	n	J	p	n
$1d_{5/2}$	$1p_{3/2}^{-1}$	0	0.000	0.000	1	−0.157	−0.010
$1d_{3/2}$	$1p_{3/2}^{-1}$	0	0.002	0.046	1	−0.041	−0.132
$2s_{1/2}$	$1p_{3/2}^{-1}$	0	0.000	0.000	1	−0.036	−0.178
$1d_{3/2}$	$1p_{1/2}^{-1}$	0	0.000	0.000	1	−0.027	−0.020
$2s_{1/2}$	$1p_{1/2}^{-1}$	0	0.009	0.792	1	0.002	1.381
$1p_{3/2}$	$1s_{1/2}^{-1}$	0	0.000	0.000	1	−0.007	0.000
$1p_{1/2}$	$1s_{1/2}^{-1}$	0	−0.017	−0.020	1	0.014	0.035

The projectile excitation data are reasonably well described in coupled channels calculations with a deformation length $\delta_2 = 2.0$ fm which is the same as that found from ^{7}Li+^{12}C at 34 MeV. All the calculations for the target excitation, for each of the models used, describe the experimental data well. The deformation lengths found from the collective studies are consistent with those found in other studies. For ^{11}B, different deformation lengths were required for the $5/2^-$ and $7/2^-$ states in the strong-coupling model, but when the weak-coupling model was used the same deformation length was found to be satisfactory for all the low-lying negative parity states. Different deformation lengths were also found for the $3/2^-$ and $5/2^-$ states of ^{13}C using the weak-coupling model, but this is consistent with other studies. Microscopic calculations were also made for the target excitation data. With the exception of the $1/2^+$ state of ^{13}C, these calculations described the data well, although sometimes there was a normalization difference between the fits and the data.

ACKNOWLEDGMENTS

This work was funded by the National Science Foundation and the State of Florida. Two of us (J.C. and A.K.A.) acknowledge the support of the University of Petroleum and Minerals.

[1]M. F. Vineyard, J. Cook, K. W. Kemper, and M. N. Stephens, Phys. Rev. C **30**, 916 (1984).
[2]J. Cook, M. N. Stephens, and K. W. Kemper, Nucl. Phys. (to be published).
[3]M. F. Vineyard, K. W. Kemper, and J. Cook, Phys. Lett. **142B**, 249 (1984).
[4]M. F. Vineyard, J. Cook, and K. W. Kemper, Phys. Rev. C **31**, 879 (1985).
[5]J. Cook, Nucl. Phys. **A445**, 350 (1985).
[6]J. Cook, M. N. Stephens, K. W. Kemper, and A. K. Abdallah, Phys. Rev. C **33**, 915 (1986).
[7]G. H. Neuschaefer, M. N. Stephens, S. L. Tabor, and K. W. Kemper, Phys. Rev. C **28**, 1594 (1983).
[8]P. Schumacher, N. Ueta, H. H. Duhn, K.-I. Kubo, and W. J. Klages, Nucl. Phys. **A212**, 573 (1973).
[9]A. F. Zeller, K. W. Kemper, D. C. Weisser, T. R. Ophel, D. F. Hebbard, and A. Johnston, Nucl. Phys. **A323**, 477 (1979).
[10]A. F. Zeller, Y.-W. Lui, R. E. Tribble, and D. M. Tanner, Phys. Rev. C **22**, 1534 (1980).
[11]G. J. C. van Niftrik, L. Lapikas, H. de Vries, and G. Box, Nucl. Phys. **A174**, 173 (1971); W. J. Vermeer, M. T. Esat, M. P. Fewell, R. H. Spear, A. M. Baxter, and S. M. Burrett, Phys. Lett. **138B**, 365 (1984).
[12]F. El-Batononi and A. A. Kresnin, Nucl. Phys. **89**, 577 (1966).
[13]M. A. M. Shahabuddin, C. J. Webb, and V. R. W. Edwards, Nucl. Phys. **A284**, 83 (1977).
[14]A. B. Clegg, Nucl. Phys. **38**, 353 (1962).
[15]S. Cohen and D. Kurath, Nucl. Phys. **73**, 1 (1965); **A101**, 1 (1967).
[16]M. A. M. Shahabuddin, Ph.D. thesis, University of London, 1973.
[17]J. F. Cavaignac, S. Jang, and D. H. Worledge, Nucl. Phys. **A243**, 349 (1975).
[18]P. D. Kunz, computer code CHUCK3 (unpublished) with modifications by J. R. Comfort (unpublished) and J. Cook (unpublished).
[19]G. R. Satchler and W. G. Love, Phys. Rep. **55**, 183 (1979).
[20]J. Cook and K. W. Kemper, Arabian J. Sci. Eng. **8**, 331 (1983).
[21]F. Petrovich, R. J. Philpott, A. W. Carpenter, and J. A. Carr, Nucl. Phys. **A425**, 609 (1984).
[22]J. Cook, K. W. Kemper, P. V. Drumm, L. K. Fifield, M. A. C. Hotchkis, T. R. Ophel, and C. L. Woods, Phys. Rev. C **30**, 1538 (1984).
[23]F. Petrovich, R. H. Howell, C. H. Poppe, S. M. Austin, and G. M. Crawley, Nucl. Phys. **A383**, 355 (1982).
[24]G. Bertsch, J. Borysowicz, H. McManus, and W. G. Love, Nucl. Phys. **A284**, 399 (1977).
[25]M. Golin, F. Petrovich, and D. Robson, Phys. Lett. **64B**, 253 (1976).
[26]A. W. Carpenter and F. Petrovich, private communication.
[27]J. Cook, Comput. Phys. Commun. **31**, 363 (1984).
[28]G. S. Blanpied, W. R. Coker, R. P. Liljestrand, G. W. Hoffmann, L. Ray, D. Madland, C. L. Morris, J. C. Pratt, J. E. Spencer, H. A. Thiessen, T. Kozlowski, N. M. Hintz, G. S. Kyle, M. A. Oothoudt, T. S. Bauer, G. Igo, R. J. Ridge, C. A. Whitten, Jr., P. M. Lang, H. Nann, and K. K. Seth, Phys. Rev. C **18**, 1436 (1978).
[29]S. K. Datta, G. P. A. Berg, and P. A. Quinn, Nucl. Phys. **A312**, 1 (1978).
[30]S. J. Seestrom-Morris, D. Dehnhard, M. A. Franey, C. L. Morris, R. L. Boudrie, and H. A. Thiessen, Phys. Rev. C **28**, 1301 (1983).
[31]P. D. Greaves, V. Hnizdo, J. Lowe, and O. Karban, Nucl. Phys. **A179**, 1 (1972).
[32]T.-S. H. Lee and D. Kurath, Phys. Rev. C **22**, 1670 (1980).
[33]S. F. Collins, G. G. Shute, B. M. Spicer, V. C. Officer, I. Morrison, K. A. Amos, D. W. Devins, D. L. Friesel, and W. P. Jones, Nucl. Phys. **A380**, 445 (1982).
[34]S. J. Seestrom-Morris, M. A. Franey, D. Dehnhard, D. B. Holtkamp, R. L. Boudrie, J. F. Amann, G. C. Idzorek, and C. A. Goulding, Phys. Rev. C **30**, 270 (1984).
[35]G. C. Ball and J. Cerny, Phys. Rev. **177**, 1466 (1969).
[36]H. Ohnuma, B. A. Brown, D. Dehnhard, K. Furukawa, T. Hasegawa, S. Hayakawa, N. Hoshino, K. Leki, M. Kabasawa, K. Maeda, K. Miura, K. Mulo, T. Nakagawa, K. Nisimura, H. Orihara, T. Suehiro, T. Tohei, and M. Yasue, Nucl. Phys. **A456**, 61 (1986).
[37]D. J. Millener and D. Kurath, Nucl. Phys. **A255**, 315 (1975).